Electrical signatures and thermal stability of interstitial clusters in ion implanted Si

J. L. Benton,[a] K. Halliburton,[b] S. Libertino,[c] and D. J. Eaglesham
Bell Laboratories, Lucent Technologies, 600 Mountain Avenue, Murray Hill, New Jersey 07974

S. Coffa
CNR-IMETEM, Stradale Primosole 50, I-95121 Catania, Italy

(Received 22 May 1998; accepted for publication 24 July 1998)

Deep level transient spectroscopy (DLTS) investigations have been used to characterize the electrical properties of interstitial clusters in ion-implanted Si. Both *n*- and *p*-type samples were implanted with 145 keV–1.2 MeV Si ions to doses of 1×10^{10}–5×10^{13} cm^{-2} and annealed at 450–750 °C. On samples annealed at temperatures above 550 °C, the residual damage is dominated by two hole traps (*B* lines) in *p*-type and five electron traps (*K* lines) in *n*-type samples. Analyses of the spectra and defect depth profiles reveal that these signatures are related to Si self-interstitial clusters, and experiments confirm that these clusters do not embody large numbers of impurities such as C, O, B, or P. Four deep level signatures exhibit similar annealing behavior, suggesting that they arise from the same defect structure. On the other hand, the remaining signatures exhibit different annealing behaviors and are tentatively associated with different cluster configurations. We have found that the thermal stability of the clusters is enhanced by either increasing the Si dose or by reducing the impurity content of the substrate. The explanation of these effects proposes that bigger and more stable clusters are formed when the concentration of free interstitials available for clustering is increased and the competing interstitial trapping at impurities is inhibited. Finally, in samples implanted at doses of $\geqslant1\times10^{13}$ cm^{-2}, most of the DLTS signals exhibit a complex and nonmonotonic annealing behavior providing evidence that the clusters can transform between electronic configurations. © *1998 American Institute of Physics.* [S0021-8979(98)01121-9]

I. INTRODUCTION

Current manufacturing processing of very large scale integrated (VLSI) Si devices relies heavily on ion implantation of dopants into Si to define junctions and tailor electrical characteristics. The newest generation of products which are both faster and smaller, and which operate at lower voltages, has forced a reduction in the thermal budget allowed in the fabrication of these devices. It becomes imperative, therefore, to understand the kinetics of formation and of dissociation of ion implantation induced defects.

An elegant series of recent experiments has lead to an understanding of transient enhanced diffusion (TED) of implanted B in Si.[1–4] In particular, transmission electron microscopy (TEM) studies of the extended or {311} defects created by ion implantation showed that interstitials stored in, and then released by, these extended defects were responsible for the enhanced diffusion of the B dopants.[5–8] These results confirmed the ''plus one'' model which predicts that upon annealing of ion implantation damage, vacancies and interstitials combine leaving excess interstitials equal in number to the total number of implanted Si ions.[9] However, TED has also been observed at doses lower than those necessary for the formation of extended defects, suggesting that an additional source of interstitials exists.[10] This source has been tentatively associated with interstitial clusters that store free interstitials in situations where extended defects are not observed, such as in low dose implants or low temperature heat treatments.[11] Atomistic simulations of ion implantation, which have been successful in describing the mechanisms of TED, predict that Ostwald ripening of interstitial clusters drives the evolution from point to extended defects, requiring the formation of interstitial clusters or precursors.[12,13]

Physical data on the formation and thermal evolution of interstitial defects are mandated to verify the simulation tools used extensively in the Si microelectronics industry and to provide a thorough understanding of the materials science controlling device characteristics. Experimental evidence of small interstitial cluster defects is limited because the clusters are below the detection limit of techniques such as Rutherford backscattering spectrometry and TEM. DLTS, a uniquely sensitive tool for characterizing defects in semiconductors, has recently provided direct evidence of interstitial clusters.[14,15]

DLTS measures the concentration of carriers—either electrons or holes—which are captured and subsequently emitted from a defect that has a level in the forbidden gap of a semiconductor. Identification of the spectral signal requires correlation with other characterization techniques or extensive experiments. Such identifications have been firmly established for point defects in silicon created by electron irradiation.[16–18] The identification of DLTS signatures re-

[a]Electronic mail: jlb@bell-labs.com
[b]Present address: University of Oklahoma, Norman, OK 73069.
[c]Permanent address, CNR-IMETEM, Stradale Primosole 50, 195121 Catania, Italy.

lated to interstitial cluster defects is presently in the beginning stages. A brief review of our current understanding will establish a platform for evaluating the data in this work.

A. Evolution of point defects into interstitial clusters

A quantitative study of the evolution of point defects into extended defects in Si ion implanted *p*-type Si provided the initial experimental evidence of signatures related to interstitial clusters. A comparison of point defect generated by both electron irradiation and Si ion implantation showed that similar vacancy pairs and interstitial–impurity as well as vacancy–impurity pairs were produced by these two processes.[19,20] After annealing at temperatures $\geqslant$450 °C, vacancies and interstitial defects recombined resulting in the complete anneal of defects in electron irradiated Si but resulting in residual interstitial-type point defects in Si implanted material.[21] In this low dose, low temperature regime (30–450 °C, $3\times10^{8}-1\times10^{10}$ Si/cm^2), the identity of the DLTS defect signatures are definitively established, so the total concentrations of vacancies and interstitials could be tabulated. It was observed after interstitial–vacancy recombination, that two to three interstitials per implanted ion remained. Therefore, the dose–temperature phase space was anchored at low values in the ''plus one'' regime where only interstitial defects remained.[22]

Further investigations at higher Si ion implantation doses and higher annealing temperatures showed a transition from interstitial point defects to more complex structures produced by interstitial clustering. The thermal stability of these new signals also suggested that small interstitial aggregates had formed. The number of interstitial defects detected by DLTS was reduced to approximately 0.3/ion as the implanted Si dose was increased to 1×10^{11} cm^{-2}, in *p*-type Si after 30 min isochronal annealing at 400 °C$\leqslant T\leqslant$500 °C.

The evolution of interstitials into large clusters was observed as doses and temperatures were increased. At Si doses of $1\times10^{10}-5\times10^{13}$ cm^{-2} and anneals of 500 °C$\leqslant T\leqslant$750 °C, the number of defects per ion was further reduced, and DLTS detected a single set of new signatures which were related to interstitial clusters.[14,15] The broadening of the DLTS spectra and the larger thermal stability of these new signals provided evidence that clusters had formed.

B. Identification of interstitial clusters in *p*-type Si

The identification of electrical signals associated with interstitial clusters provides a powerful tool to examine the mechanisms of interstitial agglomeration and to characterize the formation and dissolution kinetics of interstitial clusters. In *p*-type Si, a single pair of DLTS defect signatures (*B* lines) were associated with interstitial clusters in Si ion implanted Si.[14] These two spectral features, $E_v+0.29$ eV and $E_v+0.48$ eV, were the only observed DLTS signals following a wide range of implantation conditions, 500–750 °C, $1\times10^{10}-5\times10^{13}$ Si/cm^2. Briefly, these *B*-line experiments provided the following important results. First, comparisons between epitaxial and Czochralski (CZ) Si showed that the *B*-line defects were composed of Si interstitials with little or no O or C present in the clusters. The DLTS spectral peaks associated with these hole traps are quite broad. This broadening, previously reported for the electrical signatures of extended defects,[23] suggested that *B* lines were not associated with point-like defects but with more complex defect structures. Furthermore, the depth profiles of the *B*-line defects precisely matched the IMSIL[24] Monte Carlo simulations of the extra implanted ions for the associated Si ion implantation conditions. And finally, the presence of *B* lines was seen at doses and temperatures where transient enhanced diffusion of B occurs without the formation of extended defects,[25] suggesting that small interstitial clusters could be an alternate source for TED.

These *B*-line signatures also occurred in a processing regime of doses and temperatures which produced TED and which did show the presence of {311} extended interstitial defects. In these situations, there was an additional DLTS signal with comparable thermal stability to {311} defects. Since the formation of {311} defects is known to occur in the plus one interstitial regime, this result provides the second anchor for the association of the *B* lines with interstitials.

In this work, we continue the DLTS investigation of implantation induced interstitial clusters, completing the catalog of signatures by investigating *n*-type Si, and we monitor the effect of impurity content and implantation dose on the kinetics of evolution and dissociation of these clusters.

II. EXPERIMENT

Three sets of *n*- and *p*-type Si substrates with a wide range of C and O impurity content were used in these experiments; epitaxial (Epi) Si with impurity concentrations [O]$<1\times10^{15}$ cm^{-3} and [C]$<1\times10^{15}$ cm^{-3}, CZ Si with [O]$=7\times10^{17}$ cm^{-3} and [C]$\leqslant1\times10^{16}$ cm^{-3}, and CZ Si with [O]$>1\times10^{18}$ cm^{-3} and [C]$\geqslant6\times10^{16}$ cm^{-3}. The epitaxial layers of 21 μm were grown on CZ substrates heavily doped with Sb for *n* type or B for *p* type. The doping levels of the probed regions of the samples ranged from 7×10^{14} to 4×10^{16} cm^{-3}. Si ions were implanted at energies of 145 keV–1.2 MeV at doses of $1\times10^{9}-5\times10^{13}$ cm^{-2}. DLTS, capacitance–voltage ($C-V$) profiling, and thermally stimulated capacitance (TSCAP) measurements were made using a Bio-Rad DL8000 spectrometer, on Schottky barriers fabricated by room temperature evaporation of either AuPd (*n* type) or Ti (*p* type). These combinations of shallow doping levels and ion implantation energies allowed measurements of the full damage profile in samples implanted at 1.2 MeV and measurements of the damage tail in samples implanted at 145 keV. All DLTS spectra reproduced in this work were measured with an instrument time constant of 9 ms. Thermal treatments were performed in a tube furnace under flowing He at temperatures of 400–750 °C followed by a fast quench.

III. RESULTS AND DISCUSSION

A. Identification of interstitial clusters in *n*-type ion implanted Si

A thorough investigation of interstitial clusters in ion implanted Si must encompass both *n*- and *p*-type Si in order to characterize both electron and hole traps. The initial

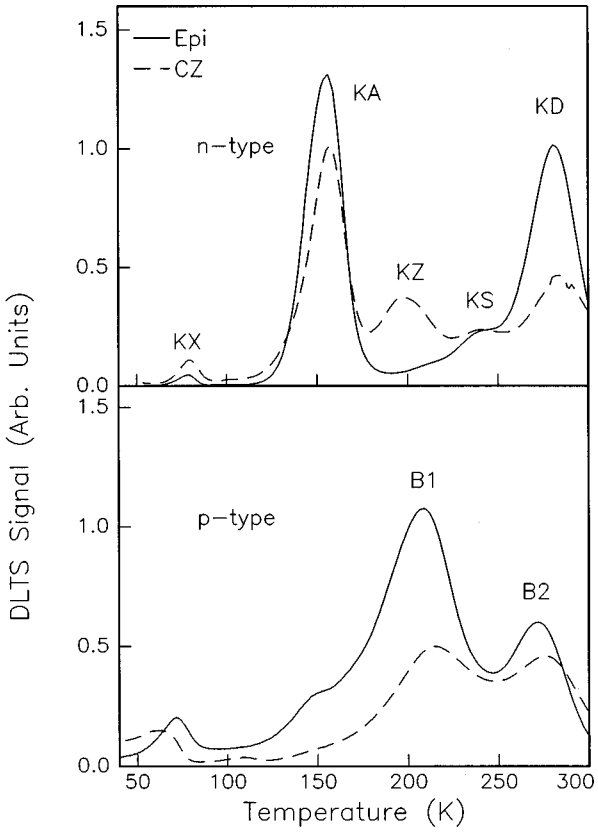

FIG. 1. DLTS spectra, $\tau_t = 9$ ms, of CZ (---) and epitaxial Si (—) implanted at 1.2 MeV, 1×10^{12} Si/cm^2 followed by a 600 °C, 30 min anneal. The *B* lines in *p*-type Si and the *K* lines in *n*-type Si are the signatures of interstitial clusters. The peak heights reflect the relative concentrations of the defects at the implant end-of-range.

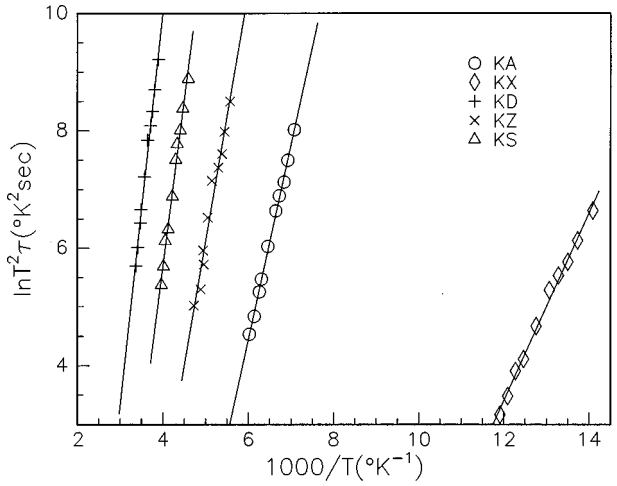

FIG. 2. Measured activation energies for thermal emission of an electron from the deep level to the conduction band for the *KA* (○), *KX* (◇), *KD* (+), *KZ* (×) and *KS* (△) defect signatures. These activation energies were measured on CZ Si, implanted with 1.2 MeV, 1×10^{12} Si/cm^2, and annealed at 600 °C, for 30 min. The values of the activation energies can change slightly with processing conditions.

DLTS experiments were measurements on *p*-type Si ion implanted Si. These data first established the boundaries of the processing parameters where interstitial cluster signals are observed. Two hole traps, $B1(E_v+0.36\text{ eV})$ and $B2(E_v+0.53\text{ eV})$ dominate the DLTS spectra in *p*-type material, although these values can vary with implant parameters.

In *n*-type Si, we find five distinct signals. Figure 1 shows the DLTS spectra measured on both CZ (dashed lines) and epitaxial (solid lines) Si following a 1.2 MeV, 1×10^{12} Si/cm^2 implant and heat treatment of 600 °C for 30 min. We observe the *B* lines in *p*-type material and the *K* lines in *n*-type Si. These unique DLTS signatures are present in Si implanted at energies from 145 keV to 2 MeV, at Si doses from 1×10^{12} to 5×10^{13} cm^{-2}, at annealing temperatures from 500 to 750 °C, and in Si samples with varying impurity concentrations, $[O]<1\times10^{15}$ cm^{-3} to $[O]\geqslant1\times10^{18}$ cm^{-3}, and $[C]<1\times10^{15}$ cm^{-3} to $[C]\geqslant6\times10^{16}$ cm^{-3}. It is interesting to note that, although large variations in cluster dimensions due to Ostwald ripening are expected within this large dose-annealing temperature range explored, the DLTS signatures do not change. This is an important result, and suggests that a single set of electrical signatures is associated with interstitial clusters having different sizes.

The usual method of describing a DLTS spectral peak is by giving the activation energy for thermal emission of a carrier from the level in the gap to the nearest band edge, or by publishing the Arrhenius plot of the emission time constant. This plot for the *K*-line defects is given in Fig. 2 for a CZ sample processed with 1.2 MeV Si at a dose of 1×10^{12} cm^{-2} and heat treated at 600 °C for 30 min. The measured activation energies are: $KX(E_c-0.14\text{ eV})$, $KA(E_c-0.29\text{ eV})$, $KZ(E_c-0.37\text{ eV})$, $KS(E_c-0.50\text{ eV})$, and $KD(E_c-0.58\text{ eV})$. For purposes of comparison with other experiments, however, it is necessary to note that the measured activation energies for the *K* lines show small changes with variations in processing conditions. This could be the result of changes in the electron capture cross section, changes in the defect environment, changes in the cluster size distribution, and/or changes in the electric field. Calculations of energy levels for *B* lines also exhibit variations. Investigations of the capture cross sections and the DLTS signal broadening for the *B* lines suggest that both hole capture at the defect and cluster size distribution are effecting the measured activation energies.[26] In this work, therefore, we have chosen to name the spectral peaks rather than identify them by their activation energies.

Research on *K* lines in *n*-type Si can now be combined with previous results on *B* lines in *p*-type material to extend our understanding of interstitial clustering in Si. We begin with an analysis of the capacitance spectra of the Si implanted *n*-type samples. As indicated in Fig. 1, *KZ* is only present in Si with high oxygen content and is not observed in the epitaxial material. All other *K* lines are present irrespective of the impurity concentration in the Si. A straightforward comparison of TSCAP (temperature dependence of the junction capacitance) with DLTS produces information about the donor or acceptor character of the *K* lines. TSCAP of the reversed biased (5 V) Schottky diode is shown with the corresponding DLTS spectra in Fig. 3 for *n*-type epitaxial Si samples implanted with 1.2 MeV Si at a dose of 1×10^{13} cm^{-2}. The samples were heated to 680 °C for three different times: 1 h (solid lines), 4 h (dashed lines), or 15 h (dot-dashed lines). After 15 h, the concentrations of defects, *KA* and *KS*, have decreased to a value of 2×10^{11} cm^{-3} and

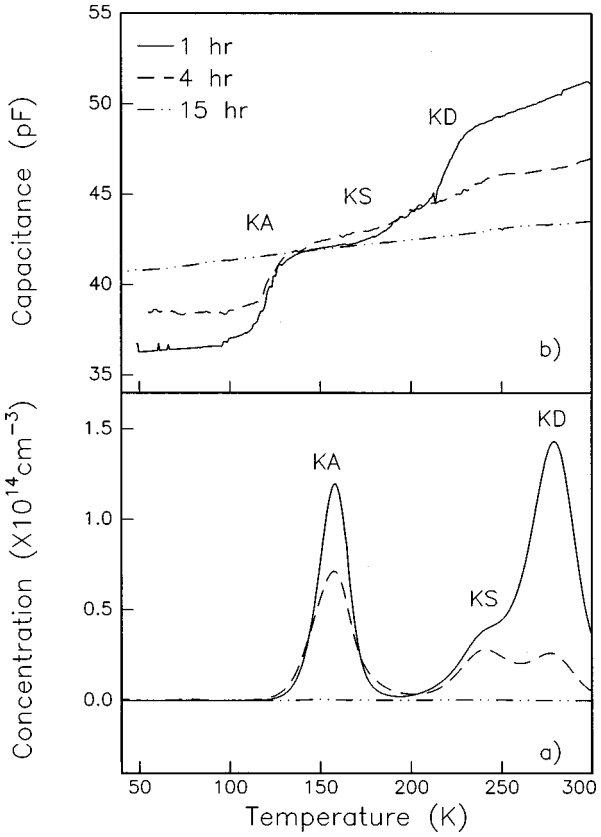

FIG. 3. DLTS spectra (a) and associated TSCAP scans (b) at a reverse bias of 5 V, measured on *n*-type epitaxial Si after a 1.2 MeV Si implant with a dose of 1×10^{13} cm^{-2} and subsequent isothermal anneal, 680 °C for 1 h (—), 4 h (---), and 15 h (·---·). *KD* and *KS* are donors, *KA* is an acceptor.

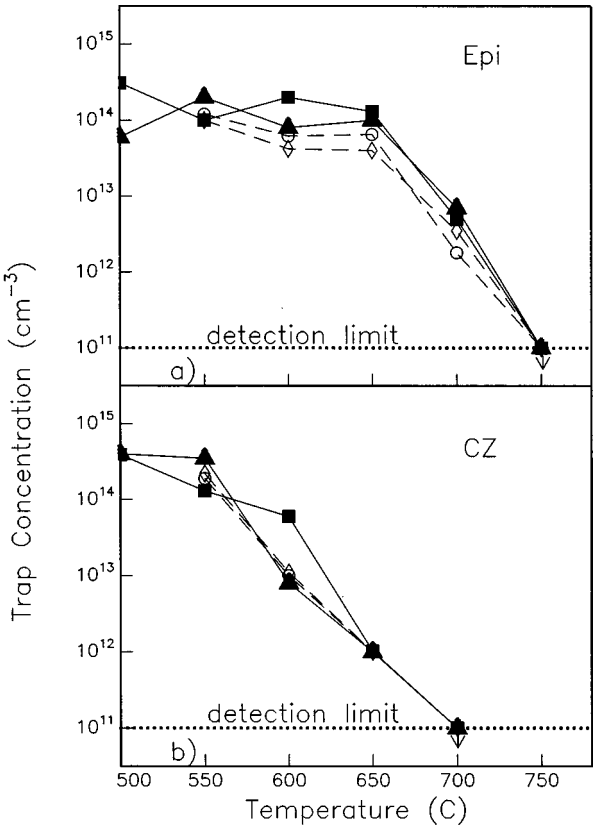

FIG. 4. Comparison of the isochronal, 30 min, annealing of DLTS signatures *KA* (■) and *KS* (▲) in *n*-type Si (—) with *B*1 (○) and *B*2 (◇) in *p*-type Si (dashed line) for epitaxial (a) and CZ (b) Si after implants of 1.2 MeV, 1×10^{12} Si/cm^2. Arrows on the data points indicate that the residual defect concentration is below the detection limit of 10^{11} cm^{-3}. The similarity of annealing characteristics suggests that *B*1, *B*2, *KA*, and *KS* are all related to the same type of defect.

defect *KD* has annealed to less than the system sensitivity limit of 1×10^{11} cm^{-3}. Therefore, this sample provides a baseline for comparison with the data taken after the two shorter anneals. The reduction in the concentration of DLTS signature *KD* corresponds to a decrease in the junction capacitance as measured by TSCAP, indicating that this defect level in the band gap is a donor. A similar analysis shows that the defect *KS* is also a donor. However, the reduction in the concentration of defect *KA* is correlated with an increase in junction capacitance denoting that this is an acceptor level.

The donor and acceptor nature of the *K* lines puts some limits on the DLTS measurements. In samples with high concentrations of ion implantation induced defects, these additional donors and acceptors change the 0-bias depletion region of the measurement diode, both as a function of temperature and of defect concentration. This means that during a single DLTS scan, the probed volume will change with measurement temperature. The measured volume will also change as the concentration of defects is changed when the implant dose is varied. Comparisons of defect concentrations cannot, therefore, be converted directly from the observed spectra. All defect concentrations presented in this work have been established by measuring the DLTS defect depth profile and determining the concentration at the maximum of the implant damage. In the cases of high defect concentrations, such as at low annealing temperatures or high Si implant doses ($\geqslant1\times10^{13}$ cm^{-2}), these values represent lower limits only.

Several DLTS signatures are observed when monitoring residual damage in both *n*-type and *p*-type samples annealed at temperatures above 550 °C, as shown in Fig. 1. In order to determine whether these signals are associated with a single defect configuration or with different defect structures, we conducted a series of isochronal annealing experiments. The resulting comparisons of the thermal stability of the defect signatures indicate that several DLTS levels seem to be related. A comparison of the concentrations of *B*1 and *B*2 in B-doped samples with *KS* and *KA* in P-doped material is presented in Fig. 4. As mentioned previously, defect concentrations plotted in this figure have been determined by taking the value of the defect concentration at the maximum of the depth profile which occurs at ~1.3 μm from the Si surface. This position is the depth of the implantation end of range for 1.2 MeV Si as simulated by the Monte Carlo code, IMSIL,[24] using an electronic stopping calibrated for high energy Si ions. The data shown in Fig. 4 are measured on Si ion implanted with 1.2 MeV 1×10^{12} Si/cm^2 after isochronal annealing for 30 mins at temperatures from 500 to 750 °C. The defects in *p*-type material (dashed lines) are *B*1 (open circles) and *B*2 (open diamonds), and the defects in *n*-type Si (solid lines) are *KA* (solid squares) and *KS* (solid triangles).

The concentration and annealing behavior of all four defect signatures is the same in epitaxial material [Fig. 4(a)]. In CZ Si, Fig. 4(b), for the same implantation parameters, these four DLTS signatures also have similar annealing kinetics. This similarity of the annealing characteristics suggests that *B*1, *B*2, *KA*, and *KS* are signatures related to identical or similar interstitial clusters. And, more importantly, this equivalence allows us to use data from both *n*- and *p*-type samples to enhance the current understanding of interstitial defect clustering. The minimum observable defect concentration for this set of experiments is 1×10^{11} cm^{-3}, so that the data points marked with arrows represent an upper limit, and complete annealing can have occurred at a lower temperature. In addition, the data reported in Figs. 4(a) and 4(b), also provide evidence that these signatures anneal at a lower temperature in CZ with respect to epitaxial Si. This interesting result will be discussed in Sec. III B.

The other defect signatures seen in *n*-type, Si ion implanted Si: *KD*, *KZ*, and *KX* of Fig. 1 have markedly different thermal evolution characteristics, as will be shown later. Therefore, they are most probably related to entirely different defects, either of different sizes, configurations, or atomic constituents. At this point, we will combine the previously published results on the *B* lines with the new measurements of *KA* and *KS* to establish that we are indeed monitoring interstitial clusters.

Two solid pieces of evidence for the identification of the *B* lines as small interstitial clusters have been previously published. First, the counting of defects/ion as a function of temperature and as a function of Si ion implantation dose shows that the vacancy and interstitial point defects recombine until only interstitial-type defects remain. The reduction in the number of defects/ion at temperatures above 450 °C and at doses above 1×10^{11} Si/cm^2 indicates that new interstitial point defects or small clusters begin to form.[15,21] The second piece of evidence that *B* lines are signals of clusters comes from careful analysis of the DLTS signatures. Both the *B*1 and *B*2 DLTS signals are broadened, and this is a spectral feature related to extended defects. Broad DLTS peaks are a consequence of a distribution in activation energies associated with extended defects, either as result of a distribution of thermal emission of carriers or a distribution of carrier capture. *K*-line peaks also show broadening after some, but not all, processing sequences. It becomes important, in this light, to show alternative data supporting the assignment of interstitial clusters to these *K*-line signatures.

An analysis of the DLTS defect depth profiles provides this evidence. In Fig. 5 we compare the depth concentration profile of a known interstitial pair point defect (the carbon interstitial–oxygen interstitial pair, C_iO_i) with that of the *KA* signal. The data are shown for two samples implanted with 1.2 MeV Si. The C_iO_i signal is measured in as-implanted Si at a dose of 1×10^{9} cm^{-2} (triangles), and the *KA* signature is measured in Si implanted at a dose of 1×10^{12} cm^{-2} and heated to 600 °C for 30 min (circles). Output from a Monte Carlo simulation, MARLOWE,[27] for this energy and ion specie is also included in Fig. 5, showing both the Frenkel pair profile (dashed line) and the extra ion profile (solid line). The depth of the Marlowe data has been scaled to reflect the end

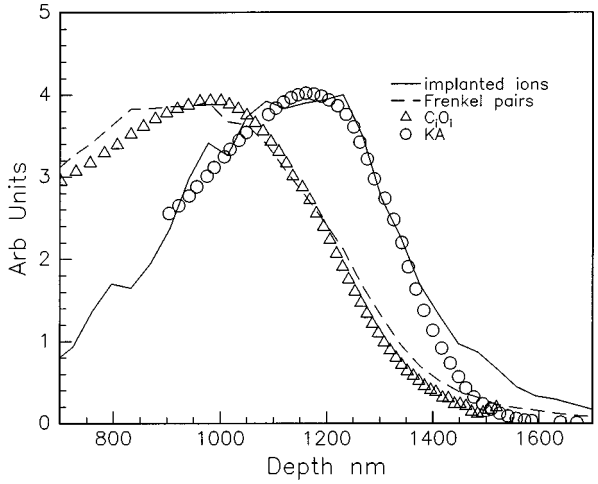

FIG. 5. DLTS depth profiles of defects created by 1.2 MeV Si ion implantation. The C_iO_i (△) point defect (1×10^{9} Si/cm^2, as implanted) distribution matches the MARLOWE simulation of the Frenkel pair profile (----). The *KA* (○) cluster defect (1×10^{12} Si/cm^2, 600 °C, 30 min) profile matches the expected implanted ions distribution (—).

of range predicted by IMSIL. At low doses, before thermal treatment, profiles of simple interstitial and vacancy defects mimic the depth distribution of the Marlowe Frenkel pairs, as illustrated in Fig. 5 for the carbon interstitial–oxygen interstitial pair, C_iO_i, $E_v+0.46$ eV. At higher doses and higher temperatures, after complete recombination of interstitial and vacancy point defects, any remaining interstitial clusters are expected to reproduce the Marlowe extra-ion profile. *B*-line defects do in fact exhibit this characteristic, as do *K* lines. The depth distribution of *KA* in *n*-type, CZ Si, following 1.2 MeV Si, 1×10^{12} cm^{-2}, 600 °C 30 mins is presented in Fig. 5 as an example. With confidence that both the *B* lines and the *K* lines are signals related to interstitial clusters, we can from here forward use data from both *n*- and *p*-type Si to investigate the thermal stability of these defects and to discover the effect of impurity content on their evolution.

B. Effect of impurities and Si implantation dose on thermal stability of clusters

Our analyses of the effect of impurities on the dissociation of interstitial aggregates begin by establishing that these impurities are not included in the interstitial clusters themselves. Further evaluation of Figs. 1 and 4 supports the conclusion that the clusters related to *B*1, *B*2, *KA*, and *KS* are composed primarily of Si interstitials with few, if any, B, P, O, or C atoms. The impurity concentrations in the epitaxial samples are [O]$<1\times10^{15}$ cm^{-3}, [C]$<1\times10^{15}$ cm^{-3}, and either [B]$=7\times10^{15}$ cm^{-3} or [P]$=7\times10^{14}$ cm^{-3}. In the CZ samples, the values are [O]$=7\times10^{17}$ cm^{-3}, [C]$\leqslant1\times10^{16}$ cm^{-3}, and either [B]$=3.5\times10^{15}$ cm^{-3} or [P]$=2\times10^{15}$cm^{-3}. Although there is an increase of almost 3 orders of magnitude in the O concentration and 1 order of magnitude in the C concentration between the epitaxial Si and the CZ material, approximately equal concentrations of the cluster defects are measured following heating at temperatures, 500 °C$\leqslant T\leqslant$600 °C. The clusters cannot therefore contain large concentrations of C and O.

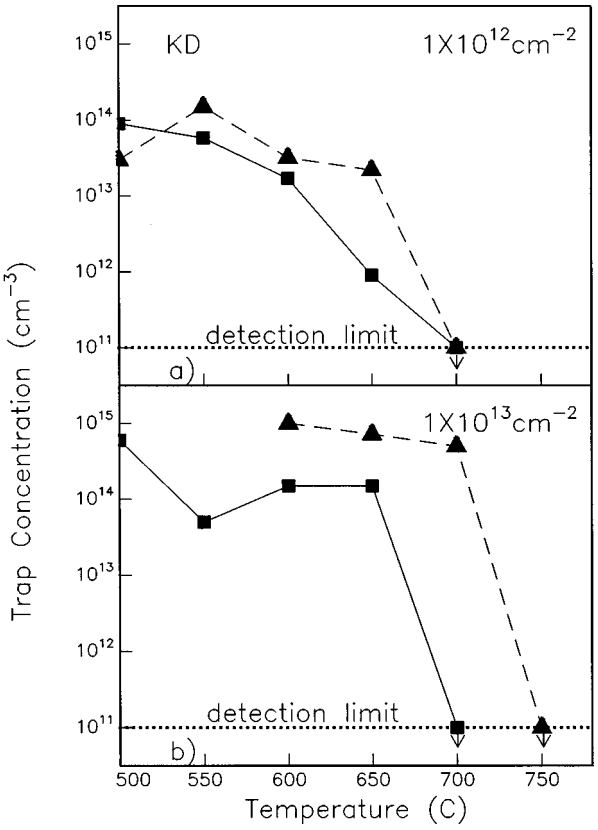

FIG. 6. Concentration of defect signature *KD* for isochronal, 30 min anneals reported for CZ (—) and epitaxial (---) Si and measured after 1.2 MeV Si implants at two doses, 1×10^{12} cm^{-2} (a) and 1×10^{13} cm^{-2} (b). The defects related to *KD* show greater thermal stability with higher dose and with lower impurity content.

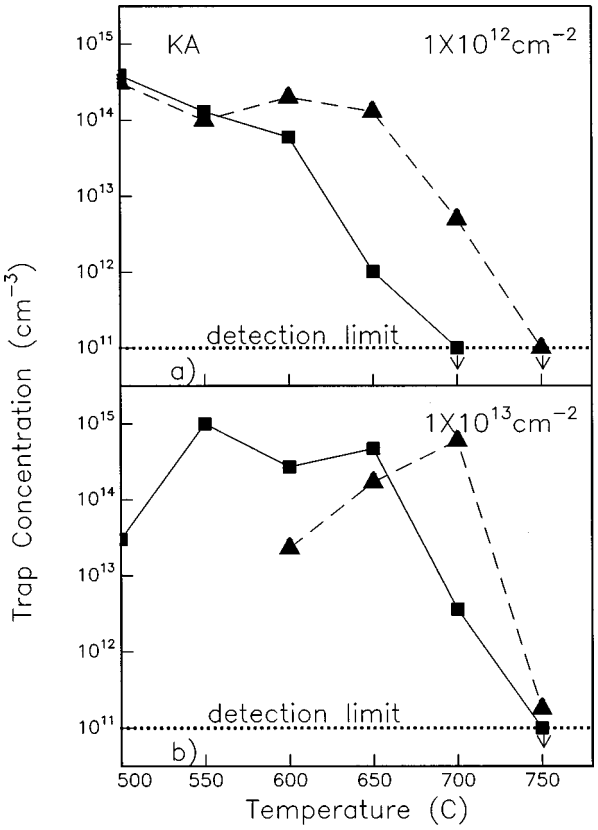

FIG. 7. Concentration of defect signature *KA* for isochronal, 30 min anneals reported for CZ (solid lines) and epitaxial (dashed lines) Si and measured after 1.2 MeV Si implants at two doses: 1×10^{12} cm^{-2} (a) and 1×10^{13} cm^{-2} (b). DLTS signals *KA*, *KS*, *B*1, and *B*2 exhibit similar trends, of increased thermal stability at higher dose and lower impurity concentrations.

The possibility of inclusion of B or P atoms in the clusters is examined by monitoring the shallow dopant depth profiles using $C-V$ measurements. In *p*-type samples, these profiles show constant boron doping throughout the implanted region, indicating that the clusters do not contain large numbers of B atoms. Although the $C-V$ profiles of our *n*-type samples sometimes show an increase of donors because of the presence of *KD* and *KS*, there is never an indication of a reduction in the phosphorus doping concentration. At temperatures below 100 K, the shallow donor depth profile is flat in the region of the Si implant. Therefore, these clusters do not contain large numbers of P atoms either.

The most pronounced effect of impurities is on the dissociation of interstitial clusters. This result is evident in Fig. 4 where the signals *B*1, *B*2, *KA*, and *KS* are more thermally stable in epitaxial Si compared with CZ. Additional data are plotted in Figs. 6 and 7. The concentrations of cluster defects *KD* and *KA*, following a series of isochronal anneals for both CZ (solid lines) and epitaxial Si (dashed lines) are compiled in these figures. Data are taken on samples receiving a dose of either 1×10^{12} Si/cm^2 [Figs. 6(a) and 7(a)] or a dose of 1×10^{13} Si/cm^2 [Figs. 6(b) and 7(b)]. If the implant variables are held constant, such as 1.2 MeV, 1×10^{12} Si/cm^2, all defects in the higher impurity CZ silicon anneal at a lower temperature than the same defects in the lower impurity epitaxial silicon. The same comparison is true for the dose of 1.2 MeV, 1×10^{13} Si/cm^2.

The effect of impurities on the thermal stability of the clusters can be understood by noting that the formation energy for pairing of interstitials and nucleation of interstitial clusters is small, so that the growth of clusters is controlled by the number of available free interstitials. In epitaxial Si, annihilation of interstitials is produced by diffusion into the bulk or to the surface. Any recaptured interstitials can contribute to Ostwald ripening of existing clusters and thus delay the dissolution of clusters. In CZ Si, the number of free interstitials is reduced by an additional mechanism. Free Si self-interstitials may be trapped by C or may form C interstitials that then become trapped by O-related defects.[28] The presence of C has been shown to reduce TED[29] of B, so that it is not unreasonable to assume that the C and O impurities in the CZ Si provide sinks for interstitials. If impurities reduce the number of available interstitials during defect formation, this would result in the creation of clusters with a smaller average size and with smaller dissociation energies, consistent with the changes in thermal stability reported in Figs. 4, 6, and 7.

It is also evident upon examination of the isochronal annealing data, that not only the O and C concentrations but the implanted Si dose also effect the thermal stability of the interstitial clusters. In Figs. 6 and 7, the signatures *KD* and *KA* anneal at a lower temperature for a dose of 1×10^{12} Si/cm^2 compared to a dose of 1×10^{13} Si/cm^2, for

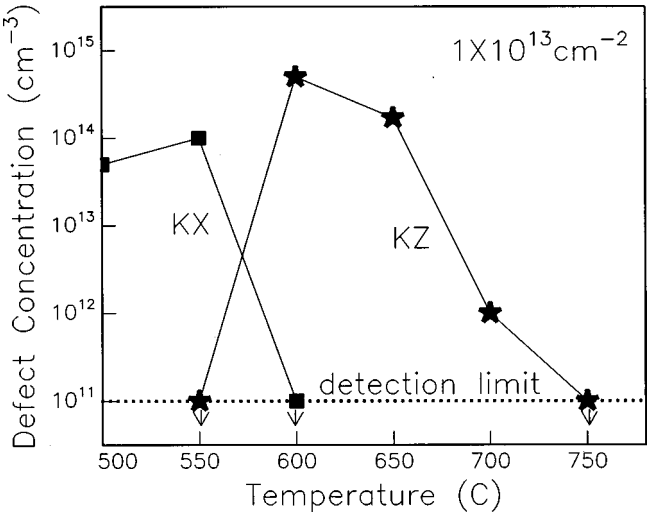

FIG. 8. Concentrations of defect signatures *KX* (■) and *KZ* (★) in CZ Si after 1.2 MeV Si ion implantation, 1×10^{13} cm^{-2}, and 30 min heat treatments. DLTS signal *KX* exhibits a transformation to signature *KZ*.

sets of samples in material of the same impurity content—that is CZ and Epi. The data for *KS* and *KZ* (in CZ Si only) are not shown, but they also exhibit the same correlation. It appears that the number of available Si interstitials, which is directly proportional to the implantation dose, determines the thermal stability of the resulting defects. Thus more interstitials produce bigger, more stable clusters. These data, along with the accompanying interpretations, suggest that the observed DLTS signals are a measure of the number rather than the size of the defect clusters. In fact, lattice reconstruction around a defect cluster is expected to result in a concentration of electrical signals much smaller than the number of defects stored in the cluster, as is the case for dislocations in Si.[30]

C. Transformation of defect configurations

We will now show that when implantation fluences are $\geqslant1\times10^{13}$ cm^{-2}, the annealing behavior of the different signatures can strongly differ from the simple monotonic behavior that we presented in the previous sections. The anomalous behavior of *KX*, shown in Fig. 8 (solid squares), is an example. At the Si implant dose of 1×10^{12} cm^{-2}, *KX* anneals in a manner consistent with the other *K* lines; however, at a dose of 1×10^{13} cm^{-2}, rather than annealing, it appears that this defect transforms to another defect configuration, *KZ* (Fig. 8, solid stars).

Further evidence, presented in Fig. 9, shows the evolution of the interstitial clusters produced by 350 keV Si at three different ion implantation doses: 1×10^{13} cm^{-2} (a), 2×10^{13} cm^{-2} (b), and 5×10^{13} cm^{-2} (c). The impurity content for this series of CZ Si samples was very high, with $[O]>1\times10^{18}$ cm^{-3}, $[C]\geqslant6\times10^{16}$ cm^{-3}, and $[P]=2\times10^{16}$ cm^{-3}. The low energy of these implants produced a shallow ion distribution and, therefore, the DLTS measurements probed only the tail of the implanted Si profile. The defect concentrations in Fig. 9 are converted from the DLTS spectral peak heights and thus represent a value averaged across the depletion depth of 400–600 nm.

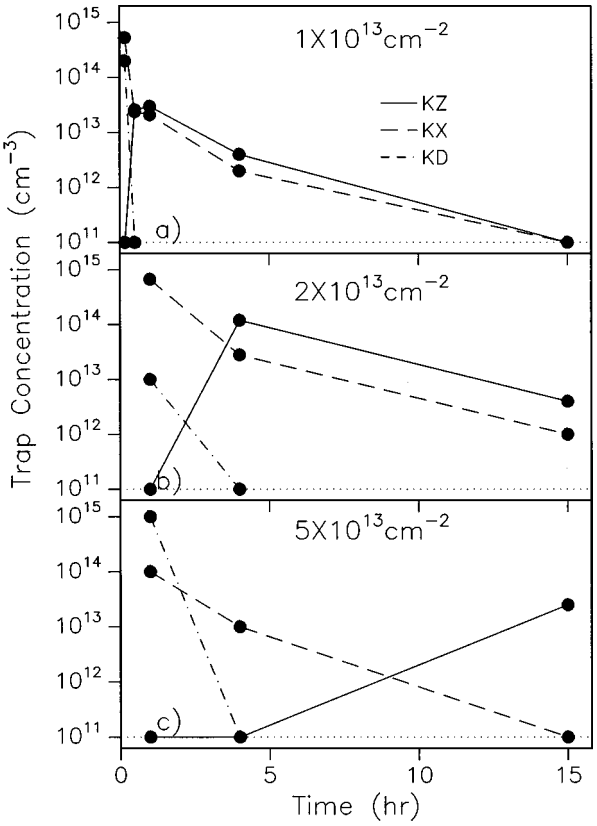

FIG. 9. Isothermal, 680 °C annealing of cluster defects *KZ* (—), *KD* (·-·-), and *KX* (---) in CZ Si implanted with 350 keV Si to doses of 1×10^{13} cm^{-2} (a), 2×10^{13} cm^{-2} (b), and 5×10^{13} cm^{-2} (c). The data suggest transformation from one defect configuration to another at all doses.

The data in Fig. 9 clearly indicate that a complex annealing behavior is exhibited by the different *K* lines. In particular, the annealing of one set of lines appears to correlate with an increase in the concentration of other lines, suggesting that defect configurations can be modified upon annealing. For the lowest dose in this set of anneals [Fig. 9(a)], signal *KZ* (solid line) is not observed after 15 min at 680 °C but grows in concentration after 30 mins. On the other hand, defect signal *KD* (dot-dashed line) exhibits a reciprocal behavior; it has annealed to below the concentration detection limit of 1×10^{11} cm^{-3} after 30 mins. This behavior presents an additional example of changes in defect configurations. A similar relation between these three cluster signatures is seen for a dose of 2×10^{13} Si/cm^2 [Fig. 9(b)], but at longer annealing times. In this case, the transformations occur between 1 and 4 h. Finally, for the highest measured dose, 5×10^{13} Si/cm^2 [Fig. 9(c)], transformation among these three *K* lines cannot provide the sole explanation of the data and new phenomena have to be taken into account.

We know from our previous TEM and DLTS studies that at the 5×10^{13} Si/cm^2 fluence, the interstitial defect evolution enters another regime that includes the growth and dissolution of extended {311} interstitial agglomerates. Published TEM micrographs show, as a function of time at 680 °C, that the concentration of these extended defects decrease while their size increases in an Ostwald ripening process, accompanied by the emission of interstitials.[7,8] These

extended {311} defects provide a source of interstitials which produces transient enhanced diffusion of boron. An associated DLTS defect signature in *p*-type Si has been correlated to the presence of {311} defects.[14] As seen in Fig. 9(c), at a dose of 5×10^{13} Si/cm^2, *KZ* (solid line) begins to increase in concentration after 4 h at 680 °C. Although not shown, *KS* and *KA* also have similar changes in thermal kinetics. These sequences of data seem to indicate that the interstitial clusters have evolved as the Si ion dose is increased, into very stable defects. In fact, the concentration of clusters appears to increase in the time–temperature regime where {311} defects are expected to undergo Ostwald ripening and emit interstitials. It may be that in addition to configurational transformation, the defects may show greater thermal stability because of equilibration with a high concentration of free interstitials; however, further experiments are necessary to fully understand the mechanism of the defect evolution in this regime.

IV. CONCLUSIONS

DLTS has provided unique measurements of interstitial cluster evolution in Si ion implanted Si, and this work has completed the catalogue of related signatures in both *n*- and *p*-type Si. Throughout a wide range of processing conditions, only the *K* lines and the *B* lines are observed and associated with interstitial clusters. Using a combination of capacitance measurements, we provide an initial identification of the *K* lines in *n*-type Si and the *B* lines in *p* type, showing that *B*1, *B*2, *KA*, and *KS* are related to the same defect clusters, and that *KZ* is related to the presence of O in the Si. *KD* and *KS* are donors and *KA* is an acceptor.

Cluster defects are formed in Si in a wide range of Si implant doses (1×10^{10}–5×10^{13} cm^{-2}), implant energies (145 keV–1.8 MeV), and heat treatments (500–750 °C). Defect depth profiles of an interstitial point defect pair (C_iO_i) and an interstitial cluster defect (*KA*) reproduce the expected distributions of vacancies and implanted ions calculated by Monte Carlo simulations, thus providing additional evidence for the identification of interstitial cluster signatures. Evidence is presented that the observed clusters contain Si self-interstitials without large concentrations of impurity atoms such as P, B, O, or C.

The thermal stability of the interstitial clusters increases upon increasing ion dose and decreasing impurity concentrations. This effect is explained by assuming that bigger and more stable clusters form when the concentration of free interstitials available for clustering is increased and the competing interstitial trapping at impurities in inhibited. Finally, in samples implanted at doses $\geqslant1\times10^{13}$ cm^{-2}, defect signatures exhibit a complex and nonmonotonic annealing behavior, providing evidence of defect configuration transformation.

ACKNOWLEDGMENTS

The authors would like to thank and acknowledge the contributions of D. C. Jacobson for his supervision of the ion implantations, and P. Kringhøj for his insight during the initial phases of this work and G. Huber and L. Pelaz for their help with the Monte Carlo simulations. This work was done while one of the authors, K. Halliburton, was an intern with Lucent.

[1] P. A. Stolk, H.-J. Gossmann, D. J. Eaglesham, D. C. Jacobson, J. M. Poate, and H. S. Luftman, Appl. Phys. Lett. **66**, 568 (1995).
[2] H.-J. Gossmann, C. S. Rafferty, H. S. Luftman, F. C. Underwald, T. Boone, and J. M. Poate, Appl. Phys. Lett. **63**, 639 (1993).
[3] P. M. Fahey, P. B. Griffin, and J. D. Plummer, Rev. Mod. Phys. **61**, 289 (1989).
[4] N. E. B. Cowern, K. T. F. Janssen, and H. F. F. Jos, J. Appl. Phys. **68**, 6191 (1990).
[5] J. K. Listebarger, K. S. Jones, and J. A. Slinkman, J. Appl. Phys. **73**, 4815 (1993).
[6] H. L. Meng, S. Prussin, M. E. Law, and K. S. Jones, J. Appl. Phys. **73**, 955 (1993).
[7] D. J. Eaglesham, P. A. Stolk, H.-J. Gossmann, and J. M. Poate, Appl. Phys. Lett. **65**, 2305 (1994).
[8] P. A. Stolk, H.-J. Gossmann, D. J. Eaglesham, D. C. Jacobson, C. S. Rafferty, G. H. Gilmer, M. Jaraiz, J. M. Poate, and T. E. Haynes, J. Appl. Phys. **81**, 6031 (1997).
[9] M. D. Giles, J. Electrochem. Soc. **138**, 1160 (1991).
[10] L. H. Zhang, K. S. Jones, P. H. Chi, and D. S. Simons, Appl. Phys. Lett. **67**, 2025 (1995).
[11] N. E. B. Cowern, G. F. A. van de Walle, P. C. Zalm, and D. W. E. Vandenhoudt, Appl. Phys. Lett. **65**, 2981 (1994).
[12] M. Jaraiz, G. H. Gilmer, J. M. Poate, and T. D. de la Rubia, Appl. Phys. Lett. **68**, 409 (1996).
[13] C. S. Rafferty, G. H. Gilmer, M. Jaraiz, D. J. Eaglesham, and H.-J. Gossmann, Appl. Phys. Lett. **68**, 2395 (1996).
[14] J. L. Benton, S. Libertino, P. Kringhøj, D. J. Eaglesham, J. M. Poate, and S. Coffa, J. Appl. Phys. **82**, 120 (1997).
[15] J. L. Benton, S. Libertino, S. Coffa, and D. J. Eaglesham, Mater. Res. Soc. Symp. Proc. **469**, 193 (1997).
[16] L. C. Kimerling, Inst. Phys. Conf. Ser. **31**, 221 (1977).
[17] M. T. Asom, J. L. Benton, R. Sauer, and L. C. Kimerling, Appl. Phys. Lett. **51**, 256 (1987).
[18] J. L. Benton, M. T. Asom, R. Sauer, and L. C. Kimerling, Mater. Res. Soc. Symp. Proc. **104**, 85 (1988).
[19] B. G. Svensson, B. Mohadjeri, A. Hallen, J. H. Svensson, and J. W. Corbett, Phys. Rev. B **43**, 2292 (1991).
[20] S. Libertino, J. L. Benton, D. C. Jacobson, D. J. Eaglesham, J. M. Poate, S. Coffa, P. Kringhøj, P. G. Fouchi, and M. Lavalle, Appl. Phys. Lett. **71**, 389 (1997).
[21] S. Libertino, J. L. Benton, D. C. Jacobson, D. J. Eaglesham, J. M. Poate, S. Coffa, P. G. Fuochi, and M. Lavalle, Mater. Res. Soc. Symp. Proc. **469**, 187 (1997).
[22] M. Jaraiz, G. H. Gilmer, J. M. Poate, and T. D. de la Rubia, Appl. Phys. Lett. **68**, 409 (1996).
[23] J. R. Ayres and S. D. Brotherton, J. Appl. Phys. **71**, 2702 (1992).
[24] G. Hobler, Nucl. Instrum. Methods Phys. Res. B **96**, 155 (1995).
[25] N. E. B. Cowern, G. F. A. Van de Walle, P. C. Zalm, and D. W. E. Vandenhoudt, Appl. Phys. Lett. **65**, 2981 (1994).
[26] S. Libertino, S. Coffa, J. L. Benton, and D. J. Eaglesham, Appl. Phys. Lett. (submitted).
[27] M. T. Robinson and I. M. Torrens, Phys. Rev. B **9**, 5008 (1974).
[28] For a complete review of oxygen precipitation in silicon see: A. Borghesi, B. Pivac, A. Sassella, and A. Stella, J. Appl. Phys. **77**, 4169 (1995).
[29] P. A. Stolk, D. J. Eaglesham, H.-J. Gossmann, and J. M. Poate, Appl. Phys. Lett. **66**, 568 (1995); Nucl. Instrum. Methods Phys. Res. B **96**, 187 (1995).
[30] L. C. Kimerling, J. R. Patel, J. L. Benton, and P. E. Freeland, Inst. Phys. Conf. Ser. **59**, 401 (1981).